

Imitation Learning with Additional Constraints on Motion Style using Parametric Bias

Kento Kawaharazuka¹, Yoichiro Kawamura¹, Kei Okada¹, and Masayuki Inaba¹

Abstract—Imitation learning is one of the methods for reproducing human demonstration adaptively in robots. So far, it has been found that generalization ability of the imitation learning enables the robots to perform tasks adaptably in untrained environments. However, motion styles such as motion trajectory and the amount of force applied depend largely on the dataset of human demonstration, and settle down to an average motion style. In this study, we propose a method that adds parametric bias to the conventional imitation learning network and can add constraints to the motion style. By experiments using PR2 and the musculoskeletal humanoid MusashiLarm, we show that it is possible to perform tasks by changing its motion style as intended with constraints on joint velocity, muscle length velocity, and muscle tension.

I. INTRODUCTION

Robots are expected to perform a variety of tasks similar to humans. For this purpose, various model-based methods [1] have been developed, while recently, methods based on deep learning have been increasing, such as reinforcement learning [2] and learning-based model predictive control [3]. Among them, imitation learning [4] learns behaviors directly from human demonstrations and thus can efficiently imitate human skills. So far, several methods have been developed, including those using image information [5], [6], and those combining force information [7]. A method with meta-learning [8] and a method with inverse reinforcement learning [9] have also been proposed.

In these imitation learning methods, the motion style such as the motion trajectory and the amount of force applied is determined depending on the dataset of human demonstrations. Usually, the imitated behavior tends to converge into an average of various human demonstrations when the imitation model is trained. However, there are cases in which we want to reproduce not only the average behavior but also the bias in the variation of human motion styles. For example, we may want to apply as little force as possible, to suppress the speed and acceleration, or to keep some joints as still as possible. Considering motion style makes it possible to change the behavior in a way that suits the current desired style. However, there are few methods which can control the motion style in imitation learning.

We summarize the methods considering motion style in imitation learning. First, there are classical methods that do not use deep learning, such as Probabilistic Movement Primitives [10], a method using Dynamic Bayesian Network

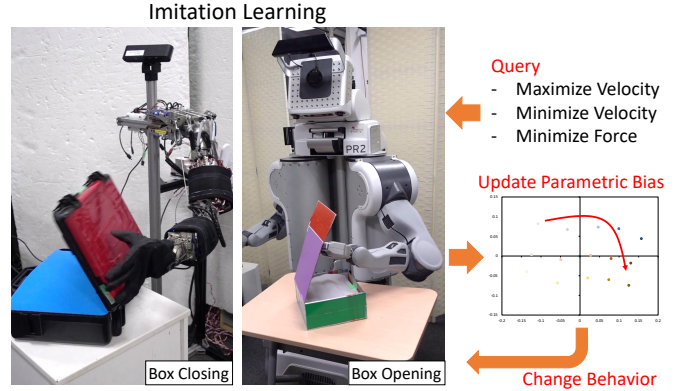


Fig. 1. Imitation learning with additional constraints on motion style.

[11], and a method using Probabilistic Principle Component Analysis [12], which can take into account additional constraints such as motion speed and obstacles. These methods make a number of assumptions about the structure of sensory and control signals, so while they can imitate behaviors from a small number of demonstrations, they are not scalable to more multi-dimensional and multi-modal systems, such as those involving raw images and tactile sensors. In contrast to these methods, InfoGAIL [13], OptionGAN [14], and MSRD [15] use reinforcement learning and inverse reinforcement learning mechanisms, and they are capable of adaptive imitation learning from raw visual information. InfoGAIL can embed differences in motion style in latent space using mutual information, OptionGAN can create policies for each motion style, and MSRD can create rewards for each motion style. On the other hand, since these motion styles are discrete values, they cannot be controlled by additional constraints. In addition, since reinforcement learning is used, they require online trials which could be costly in robotic applications.

In this study, we propose an imitation learning method that can control motion style using parametric bias [16] (Fig. 1). So far, parametric bias has been used for the purpose of extracting multiple attractor dynamics. These methods have been used to extract the dynamics of objects from multi-modal sensors [17], to extract the differences in the dynamics of object manipulation [18], and to extract the changes in the dynamics of the end effector due to tool grasping [19]. In the imitation learning process, once the multiple attractor dynamics have been trained, the human shows a robot a behavior to be imitated, the robot determines the attractor dynamics to match it, and reproduces the imitation behavior. Based on these research, we develop a novel method that

¹ The authors are with the Department of Mechano-Informatics, Graduate School of Information Science and Technology, The University of Tokyo, 7-3-1 Hongo, Bunkyo-ku, Tokyo, 113-8656, Japan. [kawaharazuka, y-kawamura, k-okada, inaba]@jsk.t.u-tokyo.ac.jp

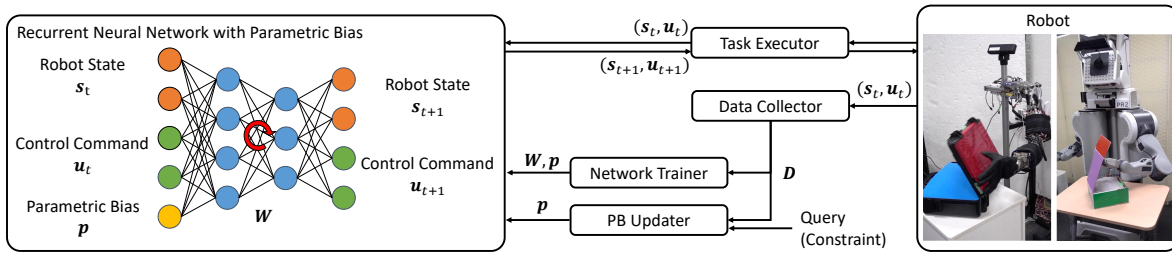


Fig. 2. The overall system of imitation learning with additional constraints.

considers additional constraints on motion style, such as motion trajectory and the amount of force applied, instead of just changing the attractor dynamics to imitate the shown behaviors. Note that the word “constraint” in this study is used as soft constraint defined by loss function, as opposed to hard constraint. By including parametric bias in common imitation learning methods with recurrent neural network [4], embedding multiple motion styles in parametric bias allows us to freely control the motion style. We validate the effectiveness of this study by experiments using a simulated 1-DOF tendon arm, the musculoskeletal humanoid MusashiLarm [20], and PR2.

This study is organized as follows. In Section II, we describe the network structure of the recurrent neural network with parametric bias, its training, task execution, and update of parametric bias considering additional constraints on motion style. In Section III, we evaluate the basic performance by a simulated 1-DOF tendon arm, and perform box opening by PR2 and box closing by a musculoskeletal humanoid MusashiLarm. Finally, the experimental results are discussed in Section IV, and the conclusion is given in Section V.

II. IMITATION LEARNING WITH ADDITIONAL CONSTRAINTS ON MOTION STYLE

We show the overall system in Fig. 2.

A. Network Structure

The recurrent neural network with parametric bias (RNNPB) used in this study, can be expressed as follows. The basic network structure is the same as [16].

$$(s_{t+1}, u_{t+1}) = h(s_t, u_t, p) \quad (1)$$

where t is the current time step, s is the sensor state, u is the control command, p is the parametric bias, and h is the function of RNNPB. s and u vary from robot to robot. For axis-driven robots, u is typically the joint angle command θ^{ref} or joint torque command τ^{ref} . Although imitation learning by a tendon-driven robot has not been done before, in this study, the muscle length command l^{ref} is used as u . The robot state s can be an arbitrary combination of sensory input such as image from camera, joint torque τ , and muscle tension f . In this study, we use z for a latent representation of camera image, which is extracted by AutoEncoder [21]. Parametric bias p is a learnable variable that is identical within a demonstration but different between different demonstrations. Each sensor value is normalized using all the obtained data and then is input to the network.

In this study, RNNPB has 10 layers, consisting of 4 fully-connected layers, 2 LSTM [22] layers, and 4 fully-connected layers in order. The number of units is set to $\{N_u + N_s + N_p, 500, 300, 100, 100\}$ (number of units in LSTM), 100 (number of units in LSTM), 100, 300, 500, $N_u + N_s$ (where $N_{\{u,s,p\}}$ is the dimension of $\{u, s, p\}$). The activation function is hyperbolic tangent and the update rule is Adam [23]. When compressing the image, for a 96×96 RGB image, the convolutional layer with kernel size 3 and stride 2 is applied five times, and the dimension is reduced to 256 and 12 by the fully connected layers, and then the image is restored by the fully connected layers and the deconvolutional layers in the same way. The batch normalization [24] and the activation function of ReLU [25] is applied to all layers except the last layer, the activation function of sigmoid is applied for the last layer, and the update rule is Adam. The dimension of p is set to be sufficiently smaller than the number of demonstrations. The execution period of Eq. 1 is set to 5Hz.

B. Training

We describe the training phase of RNNPB. For the simulation, a robot performs predetermined motions, and for the actual robot, a human teaches a task to the robot using motion capture, VR device, etc., and obtains the data of s and u at that time. For k -th demonstration of the task, we obtain the data $D_k = \{(s_1, u_1), (s_2, u_2), \dots, (s_{T_k}, u_{T_k})\}$ ($1 \leq k \leq K$, where K is the total number of demonstrations and T_k is the number of time steps for the demonstration k). Then, we obtain the data $D_{train} = \{(D_1, p_1), (D_2, p_2), \dots, (D_K, p_K)\}$ for training. p_k is the parametric bias for the demonstration k , a vector that has the same value throughout one demonstration and has a different value in each demonstration. RNNPB is trained using this data D_{train} . In the training phase, we set p_k as trainable variables as well as the network weight W , i.e., we update not only W as in the usual imitation learning but also p_k at the same time. Note that the loss function for training is the mean squared error between obtained and predicted network outputs, and all p_k are optimized with the initial value of 0.

In the usual imitation learning, the average behavior among the obtained demonstrations is executed, but in this study, p_k reflects the motion style of the human for the demonstration k . For example, when manipulating an object, the position of the elbow and the speed of task execution are different for each person. Therefore, by controlling p , it is possible to control motion style, though within the range of variation of human demonstrations. It should be noted

that, although the actual motion style may change during the course of the demonstration even within one demonstration k , in this study, all motion styles in one demonstration are considered as one motion style.

In the same way, \mathbf{p} allows us to take into account the change in robot configurations such as muscle friction and muscle route due to the irreproducibility of initialization and deterioration over time [18], which is not the main topic of this study but is often observed in flexible bodies such as musculoskeletal humanoids. This enables the robot to continue moving correctly considering the sequential changes in the body. By acquiring data while changing the robot configuration, we can embed these changes into the parametric bias. At task execution, we can add constraints to make the network match the current robot configuration by changing \mathbf{p} .

C. Task Execution and Update of Parametric Bias

The method of task execution is simple. All we have to do is to obtain the current sensor state \mathbf{s}_t and control command \mathbf{u}_t , input them into Eq. 1 to obtain \mathbf{u}_{t+1} , and send it to the actual robot.

The parametric bias is updated either offline or online at the same time as the task is executed. In this study, the difference in parametric bias due to the change in robot configuration as described in Section II-B is denoted as (A), and the difference in parametric bias due to the variation of the motion style in human demonstrations is denoted as (B). For (A), since the state transition model ($(\mathbf{s}_t, \mathbf{u}_t) \rightarrow \mathbf{s}_{t+1}$) changes by the change in the robot configuration, \mathbf{p} is updated to match the predictive models of Eq. 1 and the actual robot from the data of (\mathbf{s}, \mathbf{u}) when the robot actually moves. For (B), we need to consider additional constraints such as minimizing muscle tension or maximizing velocity. This means that (A) directly affects the task achievement, while (B) is a null space of the task achievement. Thus, once we execute the task with $\mathbf{p} = \mathbf{0}$ and the data $D = \{(\mathbf{s}_1^{data}, \mathbf{u}_1^{data}), (\mathbf{s}_2^{data}, \mathbf{u}_2^{data}), \dots, (\mathbf{s}_T^{data}, \mathbf{u}_T^{data})\}$ is obtained (T is the number of time steps), we update \mathbf{p} by defining the loss functions for A and B as follows,

$$L = \|\mathbf{s}_{2:T}^{data} - \mathbf{s}_{2:T}^{pred}\|_2 + \alpha L_{constraint}(\mathbf{x}_{2:T}^{pred}) \quad (2)$$

where $\|\cdot\|_2$ is L2 norm, \mathbf{x} is $(\mathbf{s}^T \quad \mathbf{u}^T)^T$, $\mathbf{x}_{a:b}$ is the sequence of \mathbf{x} between $[a, b]$ time steps, $\mathbf{s}_{2:T}^{pred}$ is the sequence of \mathbf{s} obtained by passing $\mathbf{x}_{1:T-1}^{data}$ through \mathbf{h} in order, α is the weight, and $L_{constraint}$ is the loss function for the additional constraint in (B). Also, $\mathbf{x}_{2:T}^{pred}$ is the value of \mathbf{x} obtained by repeating the autoregressive process, passing \mathbf{x}_1^{data} through \mathbf{h} , and inputting the output into \mathbf{h} recursively. The first term on the right-hand side of Eq. 2 is the loss for (A), where the output \mathbf{u}_{t+1} from Eq. 2 is ignored and \mathbf{p} is updated to minimize the error of the predictive model of \mathbf{s} . The second term on the right-hand side of Eq. 2 is the loss for (B), where since \mathbf{u}_{t+1} changes as \mathbf{p} changes, only the initial value of data D is used and the calculation must proceed autoregressively. If we take the loss only for (B), we do not need to execute

the task, and only the current state $(\mathbf{s}_1^{data}, \mathbf{u}_1^{data})$ is needed to be given. There are various possible definitions for $L_{constraint}$, examples of which are shown below,

$$L_{constraint}^{tension} = \|\mathbf{f}_{2:T}^{pred}\|_2 \quad (3)$$

$$L_{constraint}^{velocity} = \|\mathbf{l}_{3:T}^{pred} - \mathbf{l}_{2:T-1}^{pred}\|_2 \quad (4)$$

$$L_{constraint}^{jvelocity} = \|\boldsymbol{\theta}_{3:T}^{pred} - \boldsymbol{\theta}_{2:T-1}^{pred}\|_2 \quad (5)$$

where \mathbf{f}^{pred} is the value of \mathbf{x}^{pred} when \mathbf{x}^{pred} contains the muscle tension \mathbf{f} , \mathbf{l}^{pred} is the value of \mathbf{x}^{pred} when \mathbf{x}^{pred} contains the muscle length \mathbf{l} , and $\boldsymbol{\theta}^{pred}$ is the value of \mathbf{x}^{pred} when \mathbf{x}^{pred} contains the joint angle $\boldsymbol{\theta}$. If we want to minimize the muscle tension, Eq. 3 is used with positive α , and if we want to increase the muscle tension and maintain the joint stiffness, Eq. 3 is used with negative α , which is also true for the velocity. We can also constrain \mathbf{p} not to converge to an undesired value by adding the term $\|\mathbf{p}\|_2$ as a constraint to Eq. 2. Since \mathbf{p}_k basically concentrates around $\mathbf{0}$, we can add a minimization constraint of \mathbf{p} to prevent it from deviating too far from $\mathbf{0}$. When updating \mathbf{p} , the network weight W is fixed and only \mathbf{p} is updated with Momentum SGD [26]. When updating the parametric bias offline, we execute the task with $\mathbf{p} = \mathbf{0}$ once and update \mathbf{p} using the data D obtained in the execution. When updating parametric bias online, \mathbf{p} is updated using the accumulated data D after the number of data N^{online} exceeds the threshold N_{thre}^{online} . The data exceeding N_{max}^{online} are discarded from the oldest ones.

In this study, as shown in Eq. 3–Eq. 5, we are only dealing with minimization and maximization of velocity and force. Theoretically, it is possible to give a certain desired value and update \mathbf{p} so that the velocity and force become close to it. However, when opening a box, for example, the speed is not always constant but largely varies even in a single demonstration. Even if a certain desired value is given, it will not be realized, and only the overall speed becomes close to the desired value. Therefore, in this study, the values are manipulated by minimization and maximization. Note that the the magnitude of the velocity and force can be roughly controlled by scaling α in Eq. 2 accordingly.

In this study, α and $L_{constraint}$ are different depending on the experiment, and $N_{thre}^{online} = 10$ and $N_{max}^{online} = 20$ are used.

III. EXPERIMENTS

A. Experimental Setup

Fig. 3 shows each of the experimental tasks to be executed.

First, we simulate a simple tendon arm with one degree of freedom and three muscles to validate the effectiveness of the proposed method. This simulates nonlinear elastic elements and the muscle friction which make the dynamics model complex. The task is a simple movement to move the joint angle from 0 to -90 degrees. The demonstration behavior is a feedback control that repeatedly updates the target joint angle and target muscle tension in the form of $\boldsymbol{\theta}_{t+1}^{ref} \leftarrow \boldsymbol{\theta}_t^{ref} + \beta(\boldsymbol{\theta}^{task} - \boldsymbol{\theta}_t)$, $\mathbf{f}_{t+1}^{ref} \leftarrow \mathbf{f}_t^{ref} + \beta(\mathbf{f}^{style} - \mathbf{f}_t^{ref})$ and sends the target muscle length to the robot in the form of $\mathbf{l}^{ref} = \mathbf{h}_{bodyimage}(\boldsymbol{\theta}^{ref}, \mathbf{f}^{ref})$ ($\boldsymbol{\theta}^{task} = -90$ [deg] represents the joint angle to be achieved, $\boldsymbol{\theta}_t$ represents the measured

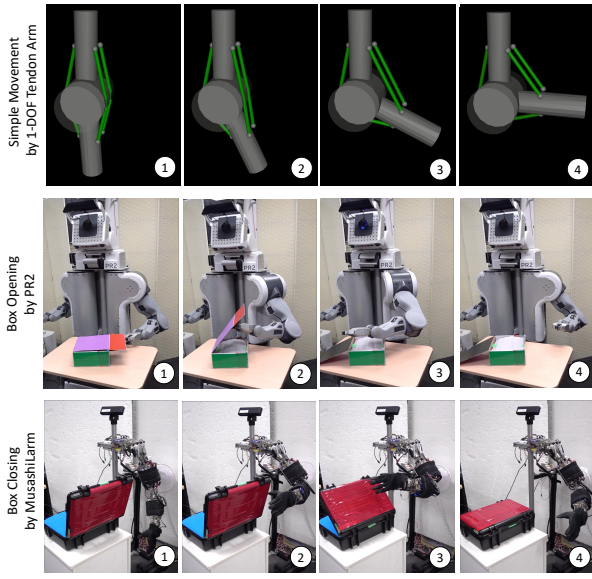


Fig. 3. Experimental setup: simple movement by 1-DOF tendon arm, box opening by PR2, and box closing by MusashiLarm.

current joint angle, \mathbf{f}^{style} represents the muscle tension to be achieved as the motion style, and β is a coefficient that represents the rate of feedback). Here, $\mathbf{h}_{bodyimage}$ is the conversion function from the target joint angle θ^{ref} and target muscle tension \mathbf{f}^{ref} to the target muscle length \mathbf{l}^{ref} learned by [27]. Note that since this model only considers the static sensor relationship, sending $\mathbf{l}^{ref} = \mathbf{h}_{bodyimage}(\theta^{task}, \mathbf{f}^{ref})$ does not directly realize θ^{task} and so this feedback control is used. The velocity and muscle tension can be adjusted by arbitrarily selecting β and \mathbf{f}^{style} , and the method is verified by varying these parameters (\mathbf{f}^{ref} can be set independently for each muscle, and the muscle tension should be set to compensate for gravity. However, in this study, the target muscle tension for all muscles is set to the same value for simplicity. The changes in β and \mathbf{f}^{style} correspond to (B) in Section II-C). In addition, by changing the joint radius r of the 1-DOF joint, i.e. the moment arm of muscles, it is possible to produce the change in robot configuration, which is (A) of Section II-C and is also used for verification. Note that in RNNPB, $\mathbf{s} = (\theta^T \mathbf{f}^T)^T$, $\mathbf{u} = \mathbf{l}^{ref}$, and \mathbf{p} is two-dimensional (in this experiment, the dimension of \mathbf{p} is set to match the dimension of the motion style of the demonstration for the sake of clarity of plots).

Next, we conduct experiments on an axis-driven dual-arm robot PR2. The task is to open a box on a table using the left arm with 7-DOF. The right arm is controlled only with the gravity compensation torque, and the left arm is controlled to send the joint angle symmetric to the right arm. When a human moves the right arm of PR2, the left arm of PR2 demonstrates the task, and imitation learning is performed. In this process, we rotate the box in various directions to obtain data. Although we used demonstration data from a single person who performed the task many times and did not add explicit perturbation, \mathbf{p} varied because the behavior of the demonstrator changed throughout the demonstrations. Note that in RNNPB, $\mathbf{s} = \mathbf{z}$, $\mathbf{u} = \theta^{ref}$ (\mathbf{z} is the image

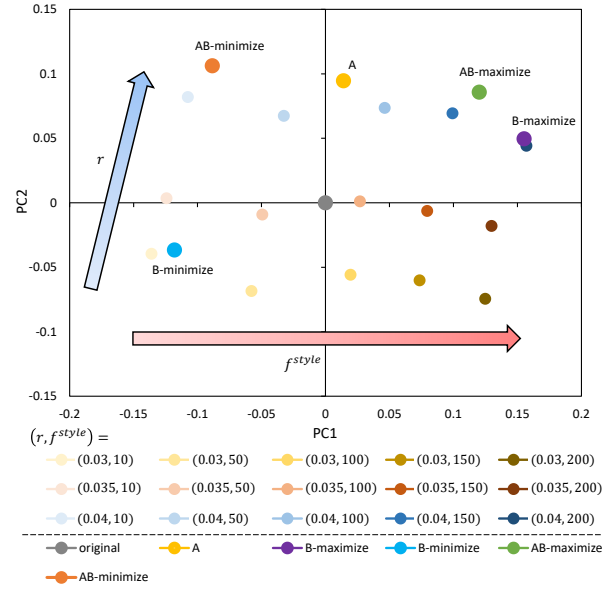


Fig. 4. Simple movement experiment by simulated 1-DOF tendon arm when changing r and \mathbf{f}^{style} : parametric biases trained in data collection phase and those updated from additional constraints regarding “A”, “B-maximize”, “B-minimize”, “AB-maximize”, and “AB-minimize”.

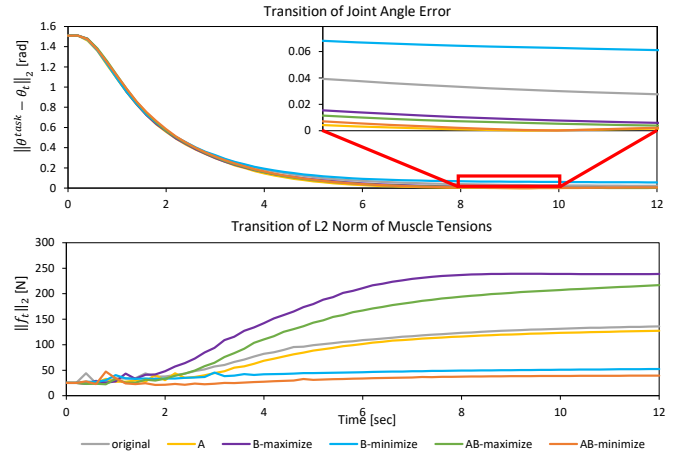


Fig. 5. Evaluation of simple movement experiment by simulated 1-DOF tendon arm when changing r and \mathbf{f}^{style} : transition of $\|\theta^{task} - \theta_i\|_2$ and $\|\mathbf{f}_i\|_2$.

compressed by AutoEncoder), and \mathbf{p} is three-dimensional.

Finally, we conduct experiments on the musculoskeletal humanoid MusashiLarm [20]. The task is to close a box on a table using the left arm with 7-DOF and 18 muscles. We obtain the hand coordinates from HTC VIVE controller, which is operated by a human, and solve inverse kinematics to obtain the target joint angle θ^{ref} , send the target muscle length by $\mathbf{l}^{ref} = \mathbf{h}_{bodyimage}(\theta^{ref}, \mathbf{f}^{ref})$, and perform the demonstration (here, we assume that $\mathbf{f}^{ref} = 10$ [N] is constant). In this process, we rotate the box in various directions to obtain data. Note that in RNNPB, $\mathbf{s} = (\mathbf{z}^T \mathbf{f}^T)^T$, $\mathbf{u} = \mathbf{l}^{ref}$, and \mathbf{p} is three-dimensional.

B. Simple Movement by Simulated 1-DOF Tendon Arm

First, experiments were conducted by varying the radius of the 1-DOF joint r and the muscle tension \mathbf{f}^{style} . For each of the 15 combinations of $r = \{0.03, 0.035, 0.04\}$ [m] and $\mathbf{f}^{style} = \{10, 50, 100, 150, 200\}$ [N], about 60 steps of

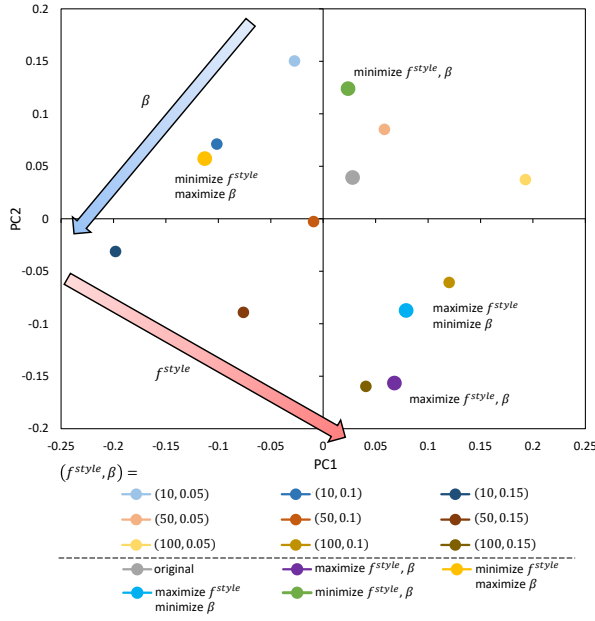


Fig. 6. Simple movement experiment by simulated 1-DOF tendon arm when changing f^{style} and β : parametric biases trained in data collection phase and those updated from additional constraints.

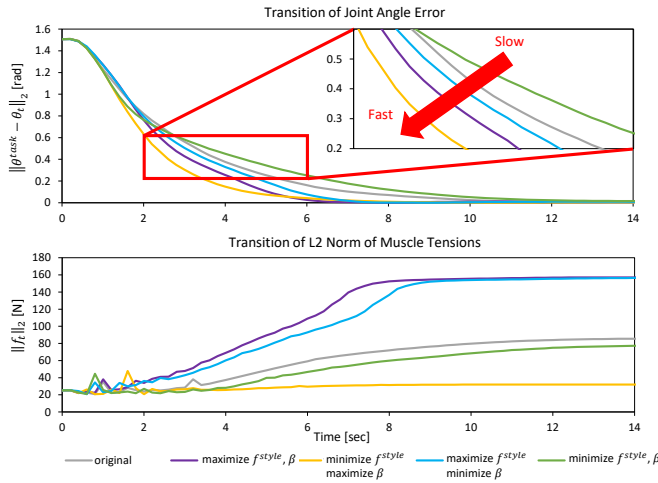


Fig. 7. Evaluation of simple movement experiment by simulated 1-DOF tendon arm when changing f^{style} and β : transition of $\|\theta^{task} - \theta_t\|_2$ and $\|f_t\|_2$.

data were obtained and used to train RNNPB. The two-dimensional representation of p_k obtained during training is shown in Fig. 4 through principle component analysis (PCA). We can see that p_k is neatly aligned along the size of r and f^{style} . In Fig. 4, we also plotted parametric biases which are updated from additional constraints by applying Eq. 2 offline denoted as, e.g. “B-minimize” or “AB-maximize”. We first executed the task with $p = \mathbf{0}$ and $r = 0.04$, and then we updated p by applying Eq. 2 with different constraints on (B). Here, the change in r corresponds to (A) in Section II-C, and the change in f^{style} corresponds to (B). We refer to the combinations of whether to include the matching constraint on (A), and whether to maximize, minimize, or not include the constraint on (B): “A”, “B-maximize”, “B-minimize”, “AB-maximize”, and “AB-minimize”. When updating p , $\alpha = 0.1$ (the sign is reversed for maximization), the learning rate

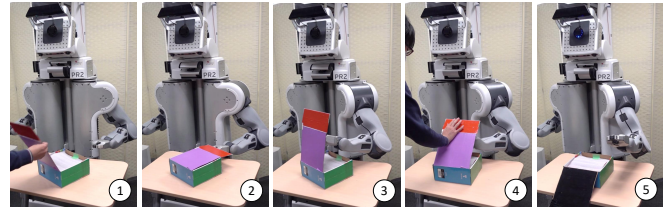


Fig. 8. The trained behavior of box opening by PR2.

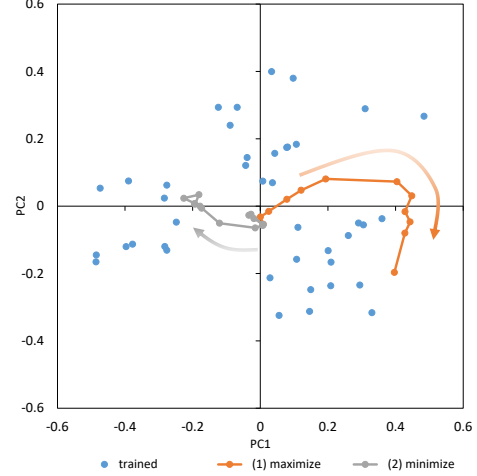


Fig. 9. Box opening experiment by PR2: parametric biases trained in data collection phase and their trajectories updated from additional constraints regarding (1) and (2).

is 0.01, the epoch is 30, and Eq. 3 is used as the loss function for (B). Also, “original” expresses $p = \mathbf{0}$ (note that $p = \mathbf{0}$ is not necessarily at the origin of the graph, since it is transformed by PCA). All p considering (A) have values close to the trained p_k at $r = 0.04$, indicating that the current value of r is correctly recognized. Also, considering (B), we can see that p has moved to the vicinity of the trained p_k at $f^{style} = 200$ [N] for maximization and to the vicinity of the trained p_k at $f^{style} = 10$ [N] for minimization. $\|\theta^{task} - \theta_t\|_2$ and $\|f_t\|_2$ during the task using p obtained here are shown in Fig. 5. Note that while p is modified continuously during online update experiments, p before and after the online update are fixed during evaluation experiments such as Fig. 5. The evaluation experiment is conducted without online update to obtain consistent graphs. For p of “original” and “B-minimize” far from the trained p_k at $r = 0.04$, θ_t does not reach θ^{task} , indicating that there is an error in achieving the task. Also, f_t is small for p that minimizes (B), f_t is large for p that maximizes (B), and f_t is somewhere in between for p with no constraint on (B). For p of “B-maximize” without the constraint on (A), we obtained p near the trained p_k at $r = 0.04$ by coincidence, and the behavior is similar to that of “AB-maximize”.

Next, the experiment was conducted by varying the muscle tension f^{style} and the coefficient β representing the motion speed ($r = 0.04$ was fixed). For each of the nine combinations of $f^{style} = \{10, 50, 100\}$ [N] and $\beta = \{0.05, 0.10, 0.15\}$, about 60 steps of data were obtained and used to train RNNPB. The two-dimensional representation of p_k obtained during training is shown in Fig. 4 through PCA. We can see that

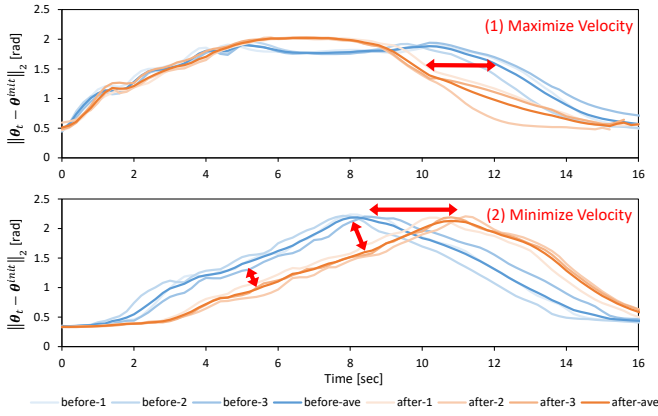


Fig. 10. Evaluation of box opening experiment by PR2: transition of $\|\theta_t - \theta^{init}\|_2$ when using \mathbf{p} before and after online update regarding (1) and (2).

\mathbf{p}_k is neatly aligned along the size of \mathbf{f}^{style} and β . The values of \mathbf{p} updated offline from additional constraints as in the previous experiment are also shown in Fig. 6. Here, we experimented with four combinations of \mathbf{f}^{style} and β , using the loss functions of Eq. 3 and Eq. 4, to maximize or minimize each of them. When updating \mathbf{p} , the weights are $(\alpha_1, \alpha_2) = (0.02, 0.3)$ (the weight for \mathbf{f}^{style} is α_1 and for β is α_2), the learning rate is 0.01, and the epoch is 30. In the following experiments, we basically consider only the constraints on (B), but we update \mathbf{p} including the matching constraint on (A) as in Eq. 2. In the axis of \mathbf{f}^{style} in Fig. 6, \mathbf{p} is updated relatively as intended by minimization and maximization. In contrast, in the axis of β , not all \mathbf{p} were updated in the intended direction. Although the desired results can be obtained by adjusting α_1 and α_2 for each optimization, it was found that careful adjustment of the ratio of weights is necessary in order to consider more than two constraints on (B). $\|\theta^{task} - \theta_t\|_2$ and $\|\mathbf{f}_t\|_2$ for the task with the obtained \mathbf{p} are shown in Fig. 7. As with the placement of \mathbf{p} on the axis of \mathbf{f}^{style} in Fig. 6, $\|\mathbf{f}_t\|_2$ can be controlled as intended by minimization and maximization in most cases. Only when both \mathbf{f}^{style} and β were minimized, \mathbf{f}^{style} was not fully minimized. For $\|\theta^{task} - \theta_t\|_2$, under the same conditions of minimizing \mathbf{f}^{style} or maximizing \mathbf{f}^{style} , the muscle length velocity was correctly modified by velocity maximization and minimization, respectively. Note that, at the time of demonstration, the antagonism increases as \mathbf{f}^{style} is increased, and the joint angle velocity is reduced with high \mathbf{f}^{style} compared to with low \mathbf{f}^{style} .

C. Box Opening by PR2

The imitated motion trained with the data of 42 demonstrations is shown in Fig. 8, and the trained \mathbf{p}_k is shown in Fig. 9. In Fig. 8, the hand withdrew when the box was opened, the hand tried to open it when it was closed, and the task was performed even when disturbed. The trajectories of \mathbf{p} when updated online with (1) maximizing or (2) minimizing the joint angle velocity using Eq. 5 at different box angles are shown in Fig. 9. By minimization and maximization, we can see that \mathbf{p} is moving in different directions. The transition of $\|\theta_t - \theta^{init}\|_2$ when the task is performed using \mathbf{p} updated by

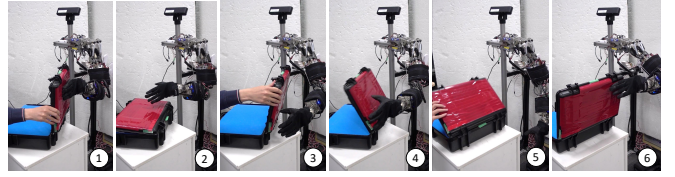


Fig. 11. The trained behavior of box closing by MusashiLarm.

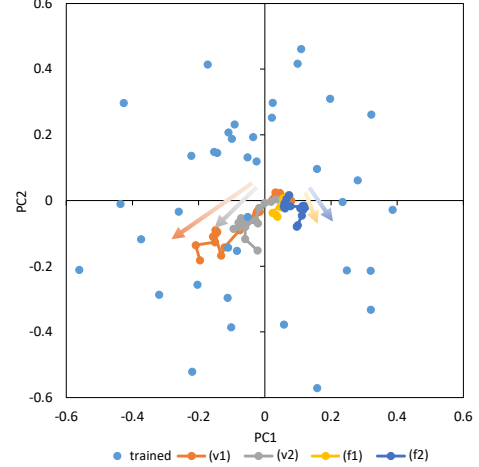


Fig. 12. Box closing experiment by MusashiLarm: parametric biases trained in data collection phase and their trajectories updated from additional constraints regarding (v1), (v2), (f1), and (f2).

(1) and (2) is shown in Fig. 10. Here we show the trajectories (“before- $\{1, 2, 3\}$ ” and “after- $\{1, 2, 3\}$ ”) and their averages (“before-ave” and “after-ave”) for the three trials before and after updating \mathbf{p} . Note that $\|\theta_t - \theta^{init}\|_2$ does not start from 0 rad, because, as a matter of convenience, we show the open box for 3 seconds and then close it to start the task. The task of opening the box was accomplished in all cases. In (1), the motion before the update of \mathbf{p} with stagnation in the middle of execution disappeared, and the robot returned to the initial posture immediately after opening the box after the update of \mathbf{p} . In (2), the motion from the first movement to the opening of the box became much slower after the update of \mathbf{p} than before.

D. Box Closing by the Musculoskeletal Arm MusashiLarm

The imitated motion trained with the data of 40 demonstrations is shown in Fig. 11, and the trained \mathbf{p}_k is shown in Fig. 12. In Fig. 11, the hand was withdrawn when the box was closed, the hand tried to close it when it was opened, and the task was performed even when disturbed. The trajectories of \mathbf{p} when updated online with maximizing muscle length velocity (v1, v2) using Eq. 4 and minimizing muscle tension (f1, f2) using Eq. 3 at different box angles (each box angle in experiment (f1), (f2), (v1), and (v2) is different) are shown in Fig. 12. We can see that \mathbf{p} is moving in the same direction in (v1) and (v2), while (f1) and (f2) do not move much from $\mathbf{p} = \mathbf{0}$. The transitions of $\|\mathbf{l}_t - \mathbf{l}^{init}\|_2$ when the task is performed using \mathbf{p} obtained in (v1) and (v2) are shown in Fig. 13. As in Section III-C, the trajectories of the three trials and their averages are shown for before and after updating \mathbf{p} . The task of closing the box was accomplished in all cases.

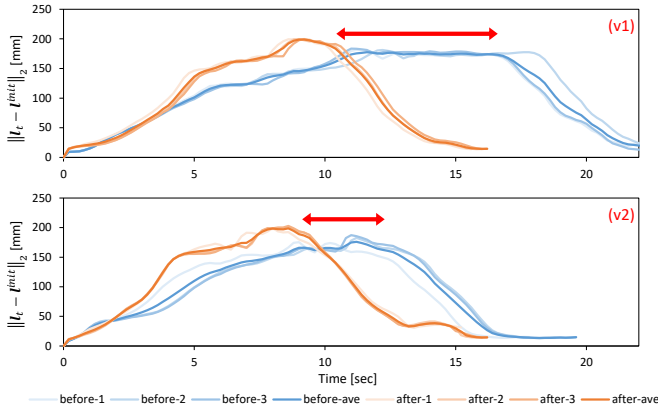


Fig. 13. Evaluation of box closing experiment by MusashiLarm: transition of $\|l_t - l^{init}\|_2$ when using p before and after online update regarding (v1) and (v2).

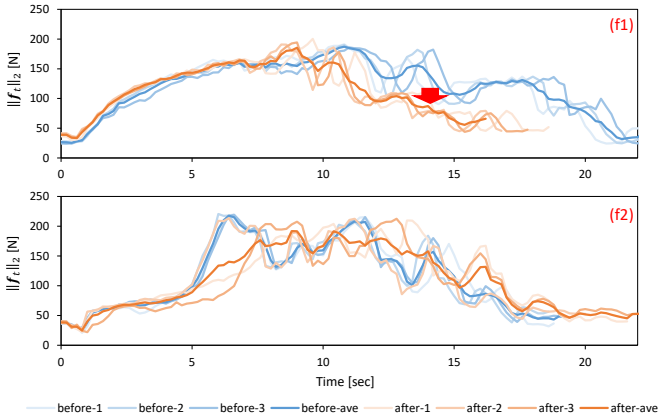


Fig. 14. Evaluation of box closing experiment by MusashiLarm: transition of $\|f_t\|_2$ when using p before and after online update regarding (f1) and (f2).

We can see that the task execution speed is greatly increased and the constraint is correctly applied. The transitions of $\|f_t\|_2$ when the task is performed using p obtained in (f1) and (f2) are shown in Fig. 14. In (f1), the muscle tension was changed to a slightly smaller motion than before the update, but in (f2), the result was not so different from before the update.

IV. DISCUSSION

First, from the simulated 1-DOF tendon arm, we found that our method can take into account the minimization and maximization constraints on muscle tension and motion speed, as well as the matching constraints on robot configuration such as the joint radius. By training RNNPB from the obtained demonstration data, p_k is neatly self-organized. By updating p to consider the constraints on the motion style and robot configuration, we can obtain p for the intended style and configuration. By using the updated p , the muscle tension and velocity during task execution could be controlled as intended. At the same time, it is difficult to adjust the ratio of the weights of loss functions when there are two or more constraints on the motion style.

Next, the box opening experiment by PR2 shows that our method can be applied to an axis-driven robot with multiple

degrees of freedom, and that p can be updated not only offline but also online. Since p is updated in the opposite direction by velocity maximization and minimization, it is considered that the information on the motion style is neatly self-organized. By actually executing the task using the obtained p , we were able to adjust the velocity as intended, demonstrating the effectiveness of this study.

Finally, the box closing experiment by MusashiLarm shows that our method can be applied to a tendon-driven robot with multiple degrees of freedom. The fact that p is updated in the same direction by velocity minimization at different box angles suggests that the information on the motion style is neatly self-organized, as in the box-opening experiment by PR2. By actually executing the task using the obtained p , we were able to adjust the velocity as intended, indicating the effectiveness of this study. On the other hand, the muscle tension could not be adjusted as intended as the velocity, but this is thought to be because there were many variations in the demonstration for the motion speed, while not much difference was obtained for the muscle tension. In this study, we did not explicitly change f^{ref} , but if we change the target muscle tension from myoelectricity of the human for example, f^{ref} will explicitly change and the constraint of the muscle tension can be considered more clearly. Although not directly related to the purpose of this study, this is the first time that a tendon-driven system with redundant muscles has been used for imitation learning, and it is expected that imitation learning utilizing a flexible body will be further developed in the future.

The limitations of this study are described as below. First, this method can only add constraints to the motion style within the range of variability obtained during the demonstration. Therefore, it is difficult to apply this method to unambiguous tasks that can only be performed in similar styles, and it is not possible to slow down the speed or reduce the power beyond the variation in the demonstration. It may be necessary to change a control device to advance a wide variety of actions during the demonstration. It is also necessary to verify how the behavior of task accomplishment changes when p deviates greatly from $\mathbf{0}$ due to unreasonable online learning, and to what extent the adaptability to human intervention, hindrance, etc., changes. Second, since the loss function cannot be defined for values that are not output from the network, this study cannot be applied to non-quantifiable behavior styles. On the other hand, if annotations are made for non-quantifiable behavioral styles, it will be possible to handle such styles by determining the desired non-quantifiable behavioral style and using parametric bias around it. Third, since the motion style of a single demonstration is embedded in a single parametric bias, it is not possible to consider the case where the style changes during the demonstration. For more complex behaviors, it is necessary to consider how to embed parametric bias when training and how to divide the demonstration data.

In this study, we mainly focused on the constraints of speed and force, but in the future, we would like to consider more constraints. For example, if an auditory sensor is added,

we can define a loss function to minimize the sound during the motion, and if a contact sensor is added, we can limit when the hand makes contact with the environment and change the applied force. We would like to aim at imitation learning using more multimodal sensors. In addition, the space of parametric bias needs to be examined in more detail in the future. It is necessary to further verify how multiple motion styles are embedded depending on the number of dimensions of parametric bias. Finally, although we have dealt with the matching constraint of robot configuration of the joint radius in the simulation, we would like to discuss whether it is possible to consider the case where the body changes due to muscle rupture or where the friction of the body increases due to deterioration over time. Although not regarding imitation learning, we have been able to capture differences in robot calibration and grasping tools by parametric bias [18], and so we would like to verify whether it is possible to take into account large changes in robot configuration, movement pattern, etc., online.

V. CONCLUSION

In this study, we proposed an imitation learning method that can take into account additional constraints on the motion style in addition to imitating the demonstrated task. The variability of the human demonstration is embedded into parametric bias. By defining loss functions for additional constraints on predictive states and control variables and updating the parametric bias offline or online, additional constraints can be considered. We have successfully applied this study to PR2 and the musculoskeletal humanoid MusashiLarm, and have succeeded in minimizing muscle tension and changing muscle length and joint velocity. In the future, we would like to consider more complex additional constraints on sound, contact force, obstacle avoidance, etc., and longer term task execution.

REFERENCES

- [1] C. Galindo, J. Fernández-Madriral, J. González, and A. Saffiotti, "Robot task planning using semantic maps," *Robotics and Autonomous Systems*, vol. 56, no. 11, pp. 955–966, 2008.
- [2] M. J. F. Zhang, J. Leitner, M. Milford, B. Upcroft, and C. Peter, "Towards vision-based deep reinforcement learning for robotic motion control," arXiv preprint arXiv:1511.03791, 2015.
- [3] K. Kawaharazuka, K. Tsuzuki, M. Onitsuka, Y. Asano, K. Okada, K. Kawasaki, and M. Inaba, "Stable Tool-Use with Flexible Musculoskeletal Hands by Learning the Predictive Model of Sensor State Transition," in *Proceedings of the 2020 IEEE International Conference on Robotics and Automation*, 2020, pp. 4572–4578.
- [4] T. Osa, J. Pajarinen, G. Neumann, J. A. Bagnell, P. Abbeel, and J. Peters, "An algorithmic perspective on imitation learning," *Foundations and Trends in Robotics*, vol. 7, no. 1-2, pp. 1–179, 2018.
- [5] P. Yang, K. Sasaki, K. Suzuki, K. Kase, S. Sugano, and T. Ogata, "Repeatable Folding Task by Humanoid Robot Worker Using Deep Learning," *IEEE Robotics and Automation Letters*, vol. 2, no. 2, pp. 397–403, 2017.
- [6] T. Zhang, Z. McCarthy, O. Jow, D. Lee, X. Chen, K. Goldberg, and P. Abbeel, "Deep Imitation Learning for Complex Manipulation Tasks from Virtual Reality Teleoperation," in *Proceedings of the 2018 IEEE International Conference on Robotics and Automation*, 2018, pp. 5628–5635.
- [7] A. Sasagawa, K. Fujimoto, S. Sakaino, and T. Tsuji, "Imitation Learning Based on Bilateral Control for HumanRobot Cooperation," *IEEE Robotics and Automation Letters*, vol. 5, no. 4, pp. 6169–6176, 2020.
- [8] C. Finn, T. Yu, T. Zhang, P. Abbeel, and S. Levine, "One-Shot Visual Imitation Learning via Meta-Learning," in *Proceedings of the 2017 Conference on Robot Learning*, 2017, pp. 357–368.
- [9] J. Ho and S. Ermon, "Generative Adversarial Imitation Learning," in *Proceedings of the 2016 Neural Information Processing Systems*, 2016, pp. 4565–4573.
- [10] A. Paraschos, C. Daniel, J. Peters, and G. Neumann, "Probabilistic movement primitives," in *Proceedings of the 2013 Neural Information Processing Systems*, 2013, pp. 2616–2624.
- [11] C. Eppner, J. Sturm, M. Bennewitz, C. Stachniss, and W. Burgard, "Imitation learning with generalized task descriptions," in *Proceedings of the 2009 IEEE International Conference on Robotics and Automation*, 2009, pp. 3968–3974.
- [12] C. A. V. Perico, J. D. Schutter, and E. Aertbeliën, "Combining Imitation Learning With Constraint-Based Task Specification and Control," *IEEE Robotics and Automation Letters*, vol. 4, no. 2, pp. 1892–1899, 2019.
- [13] Y. Li, J. Song, and S. Ermon, "Infogail: Interpretable imitation learning from visual demonstrations," in *Proceedings of the 2017 Neural Information Processing Systems*, 2017, pp. 3812–3822.
- [14] P. Henderson, W. Chang, P. L. Bacon, D. Meger, J. Pineau, and D. Precup, "Optiongan: Learning joint reward-policy options using generative adversarial inverse reinforcement learning," in *Proceedings of the 32nd AAAI Conference on Artificial Intelligence*, 2018.
- [15] L. Chen, R. Paleja, M. Ghuy, and M. Gombolay, "Joint Goal and Strategy Inference across Heterogeneous Demonstrators via Reward Network Distillation," in *Proceedings of the 2020 ACM/IEEE International Conference on Human-Robot Interaction*, 2020, pp. 659–668.
- [16] J. Tani, "Self-organization of behavioral primitives as multiple attractor dynamics: a robot experiment," in *Proceedings of the 2002 International Joint Conference on Neural Networks*, 2002, pp. 489–494.
- [17] T. Ogata, H. Ohba, J. Tani, K. Komatani, and H. G. Okuno, "Extracting multi-modal dynamics of objects using RNNPB," in *Proceedings of the 2005 IEEE/RSJ International Conference on Intelligent Robots and Systems*, 2005, pp. 966–971.
- [18] K. Kawaharazuka, K. Tsuzuki, M. Onitsuka, Y. Asano, K. Okada, K. Kawasaki, and M. Inaba, "Object Recognition, Dynamic Contact Simulation, Detection, and Control of the Flexible Musculoskeletal Hand Using a Recurrent Neural Network With Parametric Bias," *IEEE Robotics and Automation Letters*, vol. 5, no. 3, pp. 4580–4587, 2020.
- [19] S. Nishide, T. Nakagawa, T. Ogata, J. Tani, T. Takahashi, and H. G. Okuno, "Modeling tool-body assimilation using second-order Recurrent Neural Network," in *Proceedings of the 2009 IEEE/RSJ International Conference on Intelligent Robots and Systems*, 2009, pp. 5376–5381.
- [20] K. Kawaharazuka, S. Makino, K. Tsuzuki, M. Onitsuka, Y. Nagamatsu, K. Shinjo, T. Makabe, Y. Asano, K. Okada, K. Kawasaki, and M. Inaba, "Component Modularized Design of Musculoskeletal Humanoid Platform Musashi to Investigate Learning Control Systems," in *Proceedings of the 2019 IEEE/RSJ International Conference on Intelligent Robots and Systems*, 2019, pp. 7294–7301.
- [21] G. E. Hinton and R. R. Salakhutdinov, "Reducing the Dimensionality of Data with Neural Networks," *Science*, vol. 313, no. 5786, pp. 504–507, 2006.
- [22] S. Hochreiter and J. Schmidhuber, "Long short-term memory," *Neural computation*, vol. 9, no. 8, pp. 1735–1780, 1997.
- [23] D. P. Kingma and J. Ba, "Adam: A Method for Stochastic Optimization," in *Proceedings of the 3rd International Conference on Learning Representations*, 2015, pp. 1–15.
- [24] S. Ioffe and C. Szegedy, "Batch Normalization: Accelerating Deep Network Training by Reducing Internal Covariate Shift," in *Proceedings of the 32nd International Conference on Machine Learning*, 2015, pp. 448–456.
- [25] V. Nair and G. E. Hinton, "Rectified Linear Units Improve Restricted Boltzmann Machines," in *Proceedings of the 27th International Conference on Machine Learning*, 2010, pp. 807–814.
- [26] N. Qian, "On the momentum term in gradient descent learning algorithms," *Neural Networks*, vol. 12, no. 1, pp. 145–151, 1999.
- [27] K. Kawaharazuka, K. Tsuzuki, S. Makino, M. Onitsuka, Y. Asano, K. Okada, K. Kawasaki, and M. Inaba, "Long-time Self-body Image Acquisition and its Application to the Control of Musculoskeletal Structures," *IEEE Robotics and Automation Letters*, vol. 4, no. 3, pp. 2965–2972, 2019.